Journal of ELECTRONIC MATERIALS, Vol. 50, No. 5, 2021
https://doi.org/10.1007/s11664-021-08788-w

ORIGINAL RESEARCH ARTICLE

Thermoelectric Properties of Ag-Doped Sb_2Te_3 Thin Films on SiO_2 and Polyimide Substrates with Rapid Thermal Annealing

SOMPORN THAOWONKAEW,[1,2] MANISH KUMAR,[3] and ATHORN VORA-UD [1,2,4]

1.—Program of Physics, Faculty of Science and Technology, Sakon Nakhon Rajabhat University, 680 Nittayo Road, Mueang District, Sakon Nakhon 47000, Thailand. 2.—Thailand Center of Excellence in Physics, Ministry of Higher Education, Science, Research and Innovation, 328 Si Ayutthaya Road, Bangkok 10400, Thailand. 3.—Centre for Advanced Materials, Organisation for Science Innovations and Research, RS Science Park, Bah 283104, India. 4.—e-mail: athornvora-ud@snru.ac.th

This work reports Ag-doped Sb_2Te_3 (A-ST) thin films synthesized by DC magnetron sputtering method onto SiO_2 (SO) and polyimide (PI) substrates based on atomic composition optimization. The effect of post-depositional rapid thermal annealing on the crystallinity, morphology, composition, and thermoelectric properties of thin films was investigated. It was found that thin films on crystalline SO substrate yielded higher crystallinity and eventually a higher thermoelectric power factor in comparison to those grown on a polyimide substrate. The maximum room-temperature power factors achieved were 0.53 mW m^{-1} K^{-2} (PI) and 3.95 mW m^{-1} K^{-2} (SO).

Key words: Ag-doped Sb_2Te_3 thermoelectric thin films, magnetron sputtering method, rapid thermal annealing

INTRODUCTION

Currently, Sb_2Te_3 is considered for high-performance thermo-electric (TE) thin films owing to its semiconductor behavior having a narrow bandgap around 0.21 eV[1] and behaving as a topological insulator. It can be transformed into both *n*-type and *p*-type semiconductors by doping with an appropriate dopant.[2] For example, Fe-doped Sb_2Te_3 induced multiple Fermi pockets, causing reduced carrier density and mobility.[3] Since the carrier density and mobility control the power factor of TE materials[4] which is related to the performance of TE materials as defined with the dimensionless figure of merit (ZT);

$$ZT = \frac{S^2T}{\rho\kappa} = \frac{(PF)T}{\kappa}, \quad (1)$$

where S, ρ, κ, and T are Seebeck coefficient, electrical resistivity, thermal conductivity, and absolute temperature, respectively. S^2/ρ is defined as the power factor (PF). Traditional thin films have usually employed different substrates such as hard-rough Al_2O_3 and $SrTiO_3$,[5,6] hard-flat glass and SiO_2,[7] and flexible-very flat polyimide.[8] Considering that flexible TE thin film is one of the new generations of TE technology, it holds potential in wearable applications.[9] It has been reported that flexible Sb_2Te_3 thin films have demonstrated a maximum PF of 0.5×10^{-3} W m^{-1} K^{-2} (at room temperature)[10] which can be improved to 2.3×10^{-3} W m^{-1} K^{-2} when the measurement temperature is raised to 373 K.[11] Doped Sb_2Te_3 material, i.e. $AgSbTe_2$ *p*-type material, was obtained from a solid solution of Ag_2Te and Sb_2Te_3[12–14] and demonstrated an interesting high ZT around 1.59 at 673 K[15] and 1.55 at 533 K.[16]

Various magnetron sputtering methods are employed for controlling the microstructure and composition of TE thin films which eventually

(Received October 24, 2020; accepted January 27, 2021; published online February 17, 2021)

dictates the TE properties.[17–20] In this work, we doped Ag into Sb_2Te_3 (Ag-doped Sb_2Te_3, or A-ST) thin films grown on SiO_2/Si wafer and polyimide substrates through a direct-current (DC) magnetron sputtering technique. The effect of rapid thermal annealing (RTA) of thin films grown on both kinds of substrates on the crystalline structure, morphology, thickness, composition, and electrical and thermoelectric properties of thin films have been presented and correlated.

EXPERIMENTAL DETAIL

A-ST thin films were prepared by a DC magnetron sputtering process onto 1-μm SiO_2/Si wafer and polyimide substrates at a target ratio of (99.99% purity) Ag:Sb:Te 1:1:2. The base pressure was below 5.5×10^{-4} Pa, and the working pressure was about 0.93 Pa with Ar gas (99.999% UHP purity) set at a flow rate of 40 sccm. The sputtering power applied to the target was varied from 30 W, 50 W, 70 W, and 90 W, whereas the sputtering time was fixed as 10 min to optimize the atomic composition of the film on the SO substrates. For uniformity, the substrate holder was rotated at 10 rpm. After the deposition, A-ST thin films grown on both substrates with the sputtering power of 50 W were annealed by a RTA process (under the vacuum state) at temperatures of 150°C, 200°C, 250°C, and 300°C for 8 min (heating step of 5°C/s). After the RTA process, the samples were analyzed for their microstructure, morphology-thickness, and atomic composition using an x-ray diffractometer (XRD; XRD6100, Shimadzu), field emission scanning electron microscope (FE-SEM; SU8030, Hitachi), and energy-dispersive x-ray spectroscopy (EDX; SU8030, Hitachi), respectively. At room temperature, TE properties (electrical resistivity ρ and Seebeck coefficient S) of the annealed thin films were measured by the ZEM-3 apparatus (ZEM-3, Advance Riko) under helium atmosphere.

RESULTS AND DISCUSSION

Figure 1 shows the microstructure and atomic composition of the as-deposited film as optimized by varying sputtering power to be applied to the target at 30 W, 50 W, 70 W, and 90 W. The microstructure and atomic composition of the as-deposited film were determined by XRD and EDX techniques. Figure 1a presents the XRD results of as-deposited thin films showing amorphous behavior, which is a common feature of sputtered material. The EDX results showed that the Ag atoms consisted of the film at a sputtering power of 50 W to be configured to optimize the Ag doping into Sb_2Te_3 as shown in Fig. 1b. Figure 2 shows the XRD patterns of A-ST thin films grown on SO and PI substrates with a sputtering power of 50 W, as a function of annealing temperature. Figure 2a displays the Sb_2Te_3 phase structure of annealed A-ST thin films on SO by the diffraction peaks of (009), (00 $\underline{13}$), and (00 $\underline{16}$)

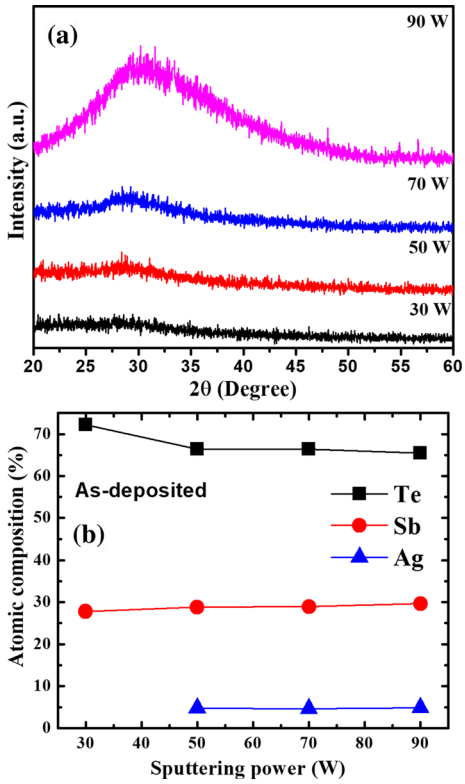

Fig 1. (a) XRD patterns and (b) atomic composition optimization of the as-deposited thin-film samples with varying sputtering power.

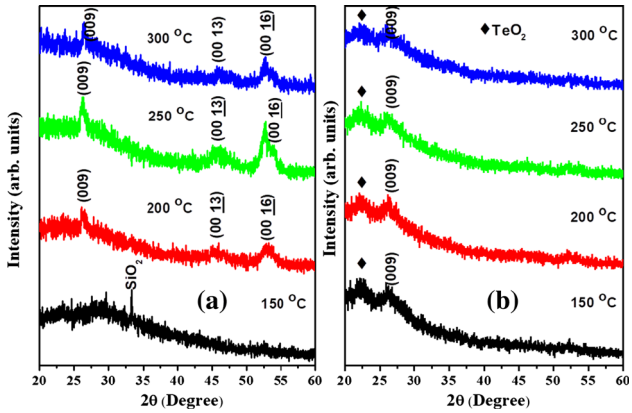

Fig 2. XRD patterns of A-ST thin films as a function of annealing temperature grown on (a) SO and (b) PI substrates.

planes, as confirmed with JCPDS 15-0727. Figure 2b displays the phase structure of annealed A-ST thin films grown on PI substrates. Here, a peak of the (009) plane was observed, assigned as the XRD peaks of the TeO_2[21] due to the partially burned surface of the polymer substrate.[22] This small hump due to TeO_2 phase is attributed to the partial surface oxidation of unsaturated Te atoms. It should be noted here that annealing in normal vacuum conditions (as used in present case) only minimizes the presence of oxygen atoms and does not completely restrain the oxygen atoms and subsequently

the chance of surface oxidation. It should be further noted that polymer substrate could also be thermally unstable during the vacuum annealing, as reported in an earlier study of Ref. 22. Such condition might lead to the diffusion of Ti atoms underneath towards the surface and therefore resulting in partial oxidation of Te. This result shows that in the case of the PI substrate, similar annealing conditions induce oxidation of thin film surface.

SEM images show the surface morphology and thickness of the A-ST thin films grown on SO and PI substrates, as shown in Fig. 3. The SEM images of as-deposited and annealed thin films correspond to (1) SO and (2) PI substrates (a) as-deposited, and annealed at (b) 150°C, (c) 200°C, (d) 250°C, and (e) 300°C. Cross-section images of thin films are inserted in corresponding SEM images. The as-deposited films demonstrate an exceptionally smooth and uniform surface morphology. It is observed that the thickness of the films decreased slightly from 260 nm (as deposited) to 173 nm (RTA at 300°C). The thickness of films decreases upon annealing due to the crystallization of material and partial re-evaporation of loosely bonded surface atoms at high annealing temperature. Also, when the temperature of RTA increases, there is an evolution of flake-like surface morphology. The surface morphology of as-deposited film illustrated a smooth surface, homogeneous morphology, and perfect adherence to the substrates. After the RTA, the morphologies of the thin films were different from that of the as-deposited sample with the grain growth and surface roughness increasing. These results confirmed that the as-deposited thin films were amorphous and then became crystalline after the temperature annealing, corresponding to the XRD results. The EDX spectra for the composition of A-ST thin films on both substrates are shown in Fig. 4, corresponding to (1) SO and (2) PI substrates (a) as-deposited, and annealed (b) 150°C, (c) 200°C, (d) 250°C and (e) 300°C. EDX results demonstrate significant contributions from the film composed of elements Ag, Sb, and Te, along with minor contributions from C, Si, and O elements for the SO substrate and C and O elements for the PI substrate.

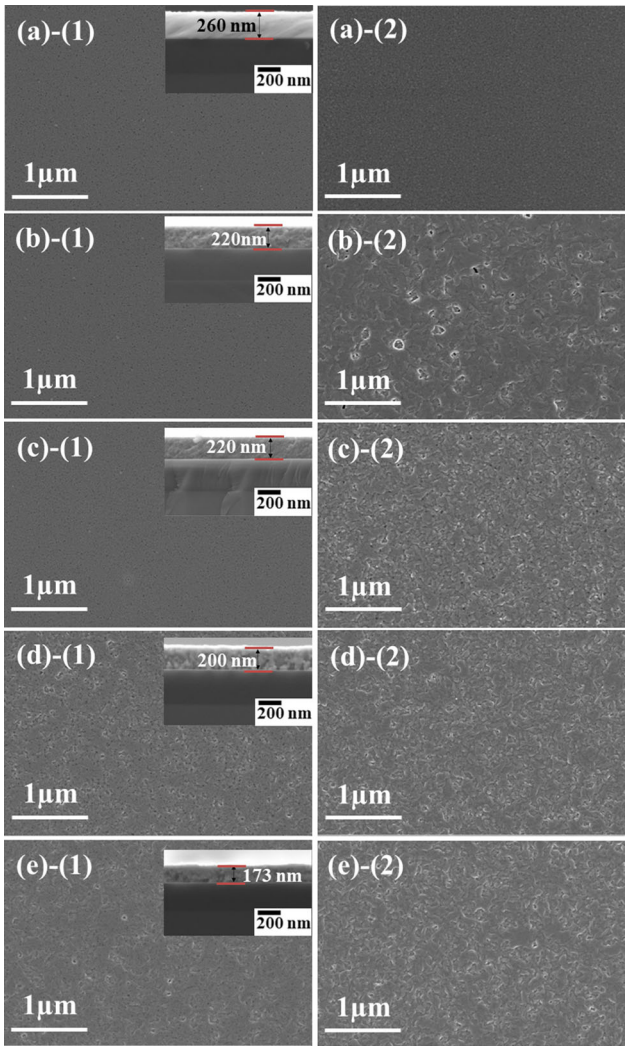

Fig 3. SEM images for surface morphology of A-ST thin films grown on (1) SO and (2) PI substrates: (a) as-deposited and annealed at (b) 150°C, (c) 200°C, (d) 250°C, and (e) 300°C. Cross sections of thin films are inserted in the corresponding SEM images.

The room-temperature thermoelectric properties (S, ρ, and P) of the A-ST thin films on SO and PI substrates are shown in Fig. 5 as a function of RTA temperatures. The annealed A-ST thin films grown on both substrates exhibited p-type thermoelectricity. The films on SO substrates had higher S values than those of the films on PI substrates at annealing temperatures of 150°C to 250°C, and then decreased slightly to exhibit similar values (of corresponding films grown on PI substrate) at an annealing temperature of 300°C. The ρ values of annealed thin films grown on SO substrates were lower than those of films grown on PI substrates for the entire range of annealing temperature. At an annealing temperature of 250°C, the lowest ρ values obtained for the thin films were 1.40×10^{-5} Ω m and 4.65×10^{-5} Ω m for the SO and PI substrates, respectively. At the same lowest electrical resistivity and annealing temperature, the A-ST thin films obtained a maximum power factor of 3.95 mW m^{-1} K^{-2} for the SO substrate and 0.53 mW m^{-1} K^{-2} for the PI substrate. The obtained power factor values of the A-ST thin films grown on the PI substrate are found comparable to the reported power factor of flexible ST thin films.[11] Moreover, the A-ST thin film on the SO substrate yielded power factors comparable to those reported for Ag-doped $Ge_2Sb_2Te_5$ thin film.[23] Such interesting power factor values suggest that these films may be used in flexible thermoelectric devices. The thermoelectric properties of films deposited on the SO substrate are better than those on the PI substrate because they yield better phase quality (purity) in comparison to the case of the PI

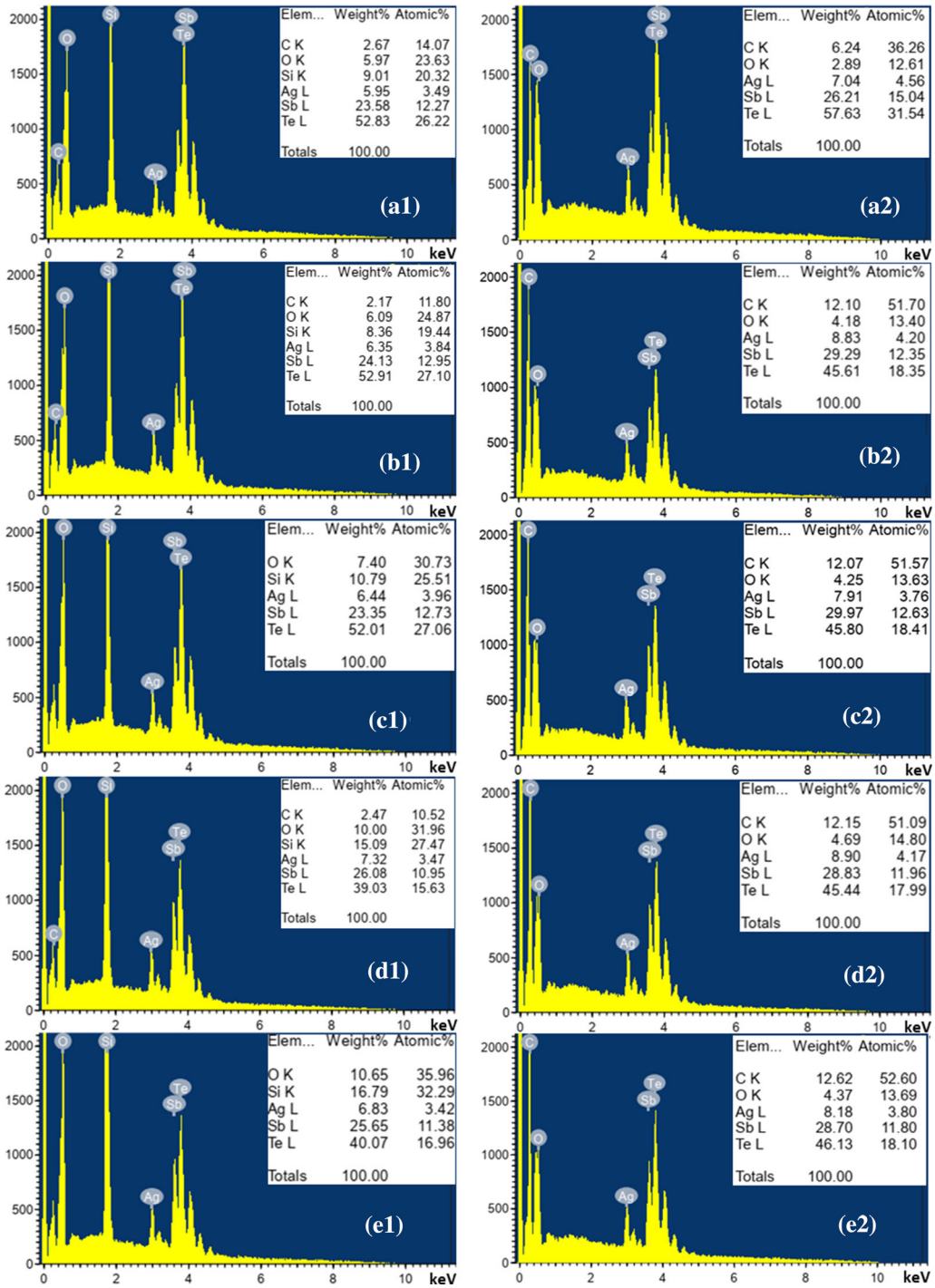

Fig 4. Atomic compositions of annealed A-ST thin films grown on (1) SO and (2) PI substrates: (a) as-deposited and annealed at (b) 150°C, (c) 200°C, (d) 250°C, and (e) 300°C.

substrate, where the thermally unstable substrate induces the surface oxidation of Te atoms.

CONCLUSION

A-ST thin films were synthesized on 1-μm SiO_2/Si-wafer and polyimide substrates by DC magnetron sputtering. The effect of the post-deposition RTA process on the microstructural and thermoelectric properties of the A-ST thin films was studied and presented. At room temperature, the maximum power factor of the A-ST thin film on the SO substrate (3.95 mW m^{-1} K^{-2}) was found to be greater than that on the PI substrate (0.53 mW m^{-1} K^{-2}), and roughly around 3.42 mW m^{-1} K^{-2} for RTA at 250°C.

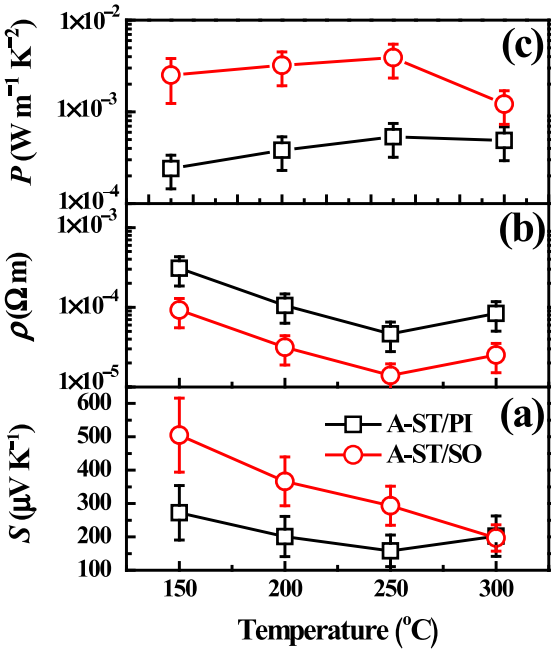

Fig 5. Thermoelectric properties: (a) *S*, (b) ρ, and (c) *P* values of A-ST thin films on SO and PI substrates as a function of the annealing temperature.

ACKNOWLEDGMENTS

This work was financially supported by the Thailand Center of Excellence in Physics.

CONFLICT OF INTEREST

On behalf of all authors, the corresponding author declares that there is no conflict of interest.

REFERENCES

1. A. Lawal, A. Shaari, R. Ahmed, and N. Jarkoni, *Results Phys.*, 2017, 7, p 2302.
2. N.N. Greenwood, and E. Alan, *Chemistry of the Elements*, 2nd edn. Butterworth-Heinemann, Oxford, 1997.
3. W. Zhao, D. Cortie, L. Chen, Z. Li, Z. Yue, and X. Wang, *Phys. Rev. B*, 2019, 99, p 165133.
4. H. Alam, and S. Ramakrishna, *Nano Enrg.*, 2013, 2, p 190.
5. A. Vora-ud, T. Seetawan, and M. Kumar, *Mater. Sci. Eng. B*, 2019, 250, p 114439.
6. P. Mele, S. Saini, H. Honda, K. Matsumoto, K. Miyazaki, H. Hagino, and A. Ichinose, Effect of substrate on thermoelectric properties of Al-doped ZnO thin films *Appl. Phys. Lett.*, 2013, 102, p 253903.
7. N. Prainetr, A. Vora-ud, S. Thaowonkaew, M. Horprathum, P. Muthitamongkol, and T. Seetawan, *Phys. B*, 2020, 582, p 411977.
8. N. Prainetr, A. Vora-ud, M. Horprathum, P. Muthitamongkol, S. Thaowonkaew, T. Santhaveesuk, T.B. Phan, and T. Seetawan, *J. Electron. Mater.*, 2020, 49, p 572.
9. S. Han, Wearable thermoelectric devices, in *Thermoelectric Thin Films*. P. Mele, D. Narducci, M. Ohta, K. Biswas, J. Morante, S. Saini, and T. Endo Eds., Springer Nature, Cham, 2019.
10. S. Shen, W. Zhu, Y. Deng, H. Zhao, Y. Peng, and C. Wang, *Appl. Surf. Sci.*, 2017, 414, p 197.
11. E.M.F. Vieira, J. Figueira, A.L. Pires, J. Grilo, M.F. Silva, A.M. Pereira, and L.M. Goncalves, *J. Alloys Compd.*, 2019, 774, p 1102.
12. H. Matsushita, E. Hagiwara, and A. Katsui, *J. Mater. Sci.*, 2004, 39, p 6299.
13. R.G. Maier, *Z. Metallkd.*, 1963, 54, p 311.
14. R.M. Marin, G. Brun, and J.C. Tedenac, *J. Mater. Sci.*, 1985, 20, p 730.
15. D.S. Song, J.O. Choi, and S.H. Ahn, *J. Electron. Mater.*, 2016, 45, p 2286.
16. J.J. Xu, H. Li, B.L. Du, X.F. Tang, Q.J. Zhang, and C. Uher, *J. Mater. Chem.*, 2010, 20, p 6138.
17. M. Kumar, A. Vora-ud, T. Seetawan, and J.G. Han, *ACS Appl. Energy Mater.*, 2018, 1, p 4025.
18. M. Kumar, A. Vora-ud, T. Seetawan, and J.G. Han, *Energy Tech.*, 2016, 4, p 375.
19. M. Kumar, A. Vora-ud, T. Seetawan, and J.G. Han, *Mater. Des.*, 2016, 98, p 254.
20. A. Vora-ud, M. Kumar, S. Jin, P. Muthitamongkol, M. Horprathum, S. Thaowonkaew, W. Chao-moo, C. Thanachayanont, P.B. Thang, T. Seetawana, and J.G. Han, *J. Alloys Compd.*, 2018, 760, p 430.
21. B. Lv, S. Hu, W. Li, X. Di, L. Feng, J. Zhang, L. Wu, Y. Cai, B. Li, and Z. Lei, *Int. J. Photoenergy*, 2010, 2010, p 1.
22. N. Somdock, A. Harnwunggmoung, A. Sakulkalavek, and R. Sakdanuphab, *Ceram. Int.*, 2019, 45, p 15860.
23. A. Vora-ud, M. Horprathum, M. Kumar, P. Muthitamongkol, C. Chananonnawathorn, B. Saekow, I. Nualkham, S. Thaowonkaew, C. Thanachayanont, and T. Seetawan, *Mater. Lett.*, 2019, 234, p 229.